Published in final edited form as:
Cell. 2014 July 3; 158(1): 198–212. doi:10.1016/j.cell.2014.04.045.

Autism-Associated Neuroligin-3 Mutations Commonly Impair Striatal Circuits to Boost Repetitive Behaviors

Marc V. Fuccillo[1,2,*], **Patrick E. Rothwell**[1,2,*], **Stephan Maxeiner**[1], **Scott J. Hayton**[2], **Ozgun Gokce**[1], **Byung Kook Lim**[2,5], **Stephen C. Fowler**[4], **Robert C. Malenka**[2], and **Thomas C. Südhof**[1,3]

[1]Department of Molecular and Cellular Physiology, Stanford University Medical School, Stanford, CA 94305

[2]Nancy Pritzker Laboratory, Department of Psychiatry and Behavioral Sciences, Stanford University Medical School, Stanford, CA 94305

[3]Howard Hughes Medical Institute, Stanford University Medical School, Stanford, CA 94305

[4]Department of Pharmacology and Toxicology, University of Kansas, Lawrence, KS 66045

Summary

In humans, neuroligin-3 mutations are associated with autism, while in mice the corresponding mutations produce robust synaptic and behavioral changes. However, different neuroligin-3 mutations cause largely distinct phenotypes in mice, and no causal relationship links a specific synaptic dysfunction to a behavioral change. Using rotarod motor learning as a proxy for acquired repetitive behaviors in mice, we found that different neuroligin-3 mutations uniformly enhanced formation of repetitive motor routines. Surprisingly, neuroligin-3 mutations caused this phenotype not via changes in the cerebellum or dorsal striatum, but via a selective synaptic impairment in the nucleus accumbens/ventral striatum. Here, neuroligin-3 mutations increased rotarod learning by specifically impeding synaptic inhibition onto D1-dopamine receptor-expressing but not D2-dopamine receptor-expressing medium spiny neurons. Our data thus suggest that different autism-associated neuroligin-3 mutations cause a common increase in acquired repetitive behaviors by impairing a specific striatal synapse, and thereby provide a plausible circuit substrate for autism pathophysiology.

Correspondence: R.C.M. (malenka@stanford.edu) or T.C.S. (tcs1@stanford.edu).
[5]Present address: Division of Biological Sciences, UC San Diego, San Diego, CA 92039
[*]Indicates equal contribution

Author contributions: MVF, PER, SM, OG, and SCF performed the experiments, SJH and GKL contributed important reagents, and MVF, PER, RCM, and TCS designed the experiments and wrote the paper.

Keywords

autism; synaptic transmission; synaptic plasticity; stereotypic behaviors; motor learning; striatum; N. accumbens; neuroligin; synaptic cell adhesion; neurexin

Introduction

Many neuropsychiatric disorders are thought to result from deficits in synaptic transmission within specific neural circuits (Akil et al., 2010). For example, genetic studies of autism spectrum disorders (ASDs) have identified multiple mutations affecting proteins that influence synaptic function (Sudhof, 2008; Zoghbi and Bear, 2012). Some of these ASD-associated mutations, when introduced into mice, cause behavioral phenotypes relevant to ASD (Etherton et al., 2009; Jamain et al., 2008; Peca et al., 2011; Tabuchi et al., 2007), providing disease models with construct and face validity (Nestler and Hyman, 2010). Our understanding of the neural circuits mediating these ASD-related phenotypes, however, remains limited. Because the inherent complexity of most neural circuits presents a daunting challenge, few studies have identified specific brain regions, cell types, and synapses where ASD-associated mutations cause dysregulation of behavior. Identification of such "molecular circuitry" represents a key step towards understanding ASD pathophysiology, and pinpointing specific synaptic connections that mediate the behavioral impact of ASD-associated mutations could allow rational design of therapeutic interventions.

The goal of the present study was to identify a robust behavioral phenotype commonly caused by different ASD-associated genetic mutations, to determine the specific brain region and cell type where these mutations alter behavior, and to search for a particular synaptic dysfunction that might account for the behavioral phenotype. To this end, we focused on neuroligin-3 (NL3), a postsynaptic cell adhesion molecule that shapes the functional properties of synapses (Sudhof, 2008). Both a deletion of NL3 (Levy et al., 2011; Sanders et al., 2011) and a point mutation of NL3 (the R451C substitution; Jamain et al., 2003) were linked to ASDs. The R451C mutation impairs intracellular trafficking of NL3 (Comoletti et al., 2004), and reduces NL3 protein levels by ∼90% (Tabuchi et al., 2007), but at the same time causes gain-of-function effects that are not observed in NL3 knockout (KO) synapses (Etherton et al., 2011; Foldy et al., 2013; Tabuchi et al., 2007). Although initially the NL3-R451C mutant phenotype was thought to be informative for ASD pathogenesis, the more recent association of the NL3 deletion with ASDs suggests that the NL3 loss-of-function phenotype may be more relevant.

No studies to date have identified behavioral phenotypes that are commonly caused by the NL3-KO and NL3-R51C mutations. Previous characterizations focused on potential deficits in social interactions (Chadman et al., 2008; Etherton et al., 2011; Radyushkin et al., 2009; Tabuchi et al., 2007), but less attention has been given to the second ASD symptom domain, which includes repetitive and stereotyped movements, routines, and rituals. Simple stereotyped movements may be innate, while more complex routines are likely acquired through repetition. Both types of behavior may involve the striatum which exhibits structural and functional alterations in ASD patients (Di Martino et al., 2011; Hollander et al., 2005;

Langen et al., 2009). Different striatal subregions interact dynamically as action sequences are repeated, and become linked in stereotyped patterns (Balleine and O'Doherty, 2010; Graybiel, 2008; Yin and Knowlton, 2006). Striatal output is processed through two discrete projections, the direct and indirect pathway, which are formed by different subtypes of medium spiny projection neurons (MSNs) with distinct anatomical and physiological properties, including differential expression of D1- and D2-dopamine receptors (D1- and D2-MSNs, respectively; Gerfen and Surmeier, 2011; Kreitzer and Malenka, 2008).

Here we show that different constitutive NL3 mutations commonly enhance acquisition of repeteitive motor routines. Using a combination of genetic tools, viral manipulations, and functional assays, we demonstrate that this phenotype is selectively recapitulated by conditional deletion of NL3 in adult nucleus accumbens (NAc), a ventral striatal subregion that functions as an interface between limbic and motor systems (Groenewegen et al., 1996). This effect was exclusively mediated by D1-MSNs in which the NL3 deletion produced a cell type-specific imbalance between synaptic inhibition and excitation. Together, our results indicate that ASD-associated NL3 mutations commonly disrupt striatal circuits in a subregion-, cell type-, and synapse-specific fashion, and suggest that this disruption may shape repetitive and stereotypic behaviors associated with ASD.

Results

Common Behavioral Phenotypes Caused by KO and R451C mutations of NL3

NL3-R451C mutant mice exhibit impaired social approach and enhanced spatial learning (Etherton et al., 2011; Tabuchi et al., 2007; but see Chadman et al., 2008), whereas NL3-KO mice exhibit impaired social memory (Radyushkin et al., 2009). However, none of these phenotypes are shared by both mouse lines, even though both mutations are linked to human ASD and the R451C mutation causes a large reduction in brain NL3 levels similar to the NL3 KO (Fig. 1A). Therefore, we sought to identify behavioral phenotypes that are common consequences of both mutations, and thus reflect a loss of NL3 function.

We noted that several mouse lines with ASD-associated mutations exhibit enhanced learning on the accelerating rotarod (Table S1), a task that requires formation and consolidation of a repetitive motor routine. We thus tested rotarod performance of NL3-KO and NL3-R451C mutant mice under “standard” conditions, with the speed of rotation accelerating from 4 to 40 rpm over 300 s (Figure 1B). On the first trial, NL3 mutant mice performed similarly to wild-type littermates (Figures 1C and 1G), and their initial performance was also similar at higher rotation speeds (Figure S1A). Over the last several trials, however, the performance of both NL3 mutant mouse lines diverged from that of wild-type mice, approaching the 300 s cutoff time. Trials are stopped at this point in standard protocols, introducing a ceiling effect that masks further improvements in performance. A substantial number of mice reached the 300 s maximum by the sixth trial, and the percentage of mice reaching maximum was higher for NL3 mutant mice than for wild-type mice (Figures 1C and 1G, insets).

To circumvent this limitation, we doubled the speed of rotarod acceleration in a second phase of the assay (Etherton et al., 2009). Under these more challenging conditions (8 to 80

rpm over 300 s), both NL3-KO and R451C mutant mice continued to improve, whereas wild-type mice showed little improvement (Figures 1D and 1H). Challenging task conditions are potentially stressful, but the continued improvement of NL3 mutant mice did not reflect enhanced ability to cope with stress as measured in the forced swim test (Figure S1B).

To better evaluate rotarod performance at both rates of acceleration, we calculated the speed of rotation at the end of each trial, and plotted this “terminal speed” across all 12 trials (Figures 1E and 1I). Significant statistical interactions between genotype and trial confirmed that superior performance developed over time in both NL3 mutant lines. We next used linear regression analyses on data from each individual mouse, and calculated the intercept (to estimate initial motor coordination) and the slope (to estimate learning rate; Figure S1C). Both NL3-KO and R451C mutant mice exhibited a significantly increased learning rate but similar initial coordination (Figures 1F and 1J). The same phenotypes were reproduced in NL3 mutant mice on a hybrid genetic background (Figure S1D-S1G), and thus are not an artifact caused by backcrossing to C57Bl/6.

To measure the consistency of the repetitive motor routine that develops during rotarod training, we analyzed videos of mice performing this task. Pilot studies identified several components of the motor routine that became less variable with training, including the vertical location of each step, the length of each step, and the time between steps (Figures 1K and S1H-S1L). To compare the consistency of these measures in wild-type and NL3-KO mice, we focused on the first and last trials at 8 to 80 rpm (i.e., trials 7 and 12), where differences in learning were most striking. During the first 30 sec of each trial, variability in each measure (represented by the standard deviation) decreased with training in NL3-KO mice (Figures 1L-1N, left panels), indicating a more repetitive motor routine. Variability in each measure also negatively correlated with time to fall off the rotarod (Figures 1L-1N, right panels), showing that the time to fall off serves as a surrogate index of this acquired repetitive behavior.

During open field tests, NL3-KO and R451C-mutant mice were consistently hyperactive (Figures 1O and 1Q), leading to significant increases in total distance travelled and in the number of ambulatory episodes for both lines of NL3 mutant mice (Figures 1P and 1R). However, there were no substantial changes in movement velocity or in crossings through the center of the open field (Figures S1M and S1N), suggesting that the rotarod phenotypes in these mice are not related to increased speed of movement or altered anxiety level.

While general hyperactivity could potentially enhance rotarod performance, this effect should be evident from the very first trial, when NL3 mutant mice perform at WT levels over a range of speeds (Figure S1A). Moreover, the open field hyperactivity and learning rates did not correlate in individual mice (Figures S1Q and S1R). Thus, these two phenotypes likely represent different facets of an underlying deficit in behavioral regulation.

We also evaluated innate forms of stereotyped behaviors during spontaneous open field activity. Both the time spent ambulatory and the time spent performing stereotypic movements were enhanced by the NL3 KO and the R451C mutation (Figures S1O-S1P).

Quantitative assessment of stereotypic movements with a force plate actometer (Fowler et al., 2001) confirmed an increased vigor of stereotypic movements in NL3-KO mice, indicated by greater force variance during periods of low mobility (Figure 1S). We also detected a greater number of wall jumps (Presti et al., 2004) and an abnormal bias in the direction of rotation during locomotion (Figures 1T and 1U). Together, these results demonstrate that ASD-associated mutations in NL3 cause a constellation of both innate and acquired behaviors that are repetitive and stereotyped.

The Molecular Circuitry of NL3-Mediated Behavioral Regulation

The results presented above indicate that two different constitutive NL3 mutations – the KO and the R451C point mutation – cause the same robust phenotypes in mouse behavioral assays of rotarod learning and open field activity. As both mutations substantially reduce NL3 protein levels (Tabuchi et al., 2007), these phenotypes are plausibly mediated by loss of NL3 in the critical brain regions and neuron types that underlie these behaviors. To interrogate this molecular circuitry, we generated NL3 conditional KO (NL3-cKO) mice in which the NL3 start codon (located in exon 2) is deleted by Cre recombinase (Figures 2A, S2A and S2B).

To confirm Cre-mediated deletion of NL3, we crossed homozygous floxed females with males carrying Nestin-Cre, which is expressed by all neurons during development. Male NL3-cKO offspring carrying Nestin-Cre showed complete loss of NL3 mRNA and protein in whole brain, with no compensatory changes in either NL1 or NL2 (Figure 2B and 2C; note that NL3 is an x-chromosomal gene). Behavioral testing of open field activity revealed the same hyperactivity phenotype as the constitutive NL3 deletion (Figures 2D and 2E).

The repetitive motor routines in NL3 mutant mice could potentially involve the cerebellum and basal ganglia, both of which are linked to motor learning (Hikosaka et al., 2002). To address the impact of deleting NL3 in specific elements of these circuits, we crossed NL3-cKO mice with transgenic mice expressing Cre in defined neuronal subpopulations. We first used L7-Cre to delete NL3 in cerebellar Purkinje cells (Figure 2F), which have been implicated in motor phenotypes caused by deletion of NL3 (Baudouin et al., 2012). We were surprised to find that this manipulation did not alter rotarod performance (Figures 2G-2J). However, NL3-cKO mice carrying L7-Cre were hyperactive (Figures 2K and 2L). Thus, despite rendering mice hyperactive, the NL3 deletion in cerebellar Purkinje cells fails to recapitulate the repetitive motor routine phenotype. We also crossed NL3-cKO mice with mice expressing Cre under the parvalbumin promoter (PV-Cre), deleting NL3 in cerebellar Purkinje cells as well as in specific populations of interneurons widely distributed throughout the brain (Fishell and Rudy, 2011). This manipulation also failed to influence rotarod performance, but significantly decreased activity in the open field (Figures S2C-S2H).

The striatum and related basal ganglia circuits contribute to the acquisition of repetitive and stereotyped behaviors (Balleine and O'Doherty, 2010; Graybiel, 2008; Yin and Knowlton, 2006), and have also been implicated in rotarod learning (Costa et al., 2004; Dang et al., 2006; Yin et al., 2009). To explore whether NL3 mutations may affect repetitive behaviors by altering striatal circuits, we used transgenic mice that express Cre in D1- or in D2-MSNs

of the striatum (Gerfen and Surmeier, 2011; Kreitzer and Malenka, 2008). When a D1-dopamine receptor-Cre line (D1-Cre) was used to delete NL3 in D1-MSNs, we observed the full spectrum of behavioral phenotypes associated with the NL3-KO and R451C mutations, namely enhancement of rotarod learning and increased open field activity (Figures 3A-3G). In contrast, when the adenosine-2a receptor-Cre line (A2a-Cre) was used to target D2-MSNs while avoiding cholinergic interneurons (Durieux et al., 2009), we detected no effect on rotarod performance or open field activity (Figures 3H-3N). Thus, ablation of NL3 in D1-MSNs alone produced the enhanced rotarod learning observed in NL3-KO mice. We also crossed D1-Cre mice with the NL3-R451C mutant line, which was generated with loxP sites flanking the mutated exon 7 (Tabuchi et al., 2007), enabling deletion of the mutant NL3-R451C protein by Cre (Figure S3A). This manipulation had no effect on the enhanced rotarod learning of NL3-R451C mutant mice (Figures S3B-S3D), as expected if the R451C mutation was already causing loss of NL3 function in these cells.

To investigate why D1-MSNs may be selectively sensitive to deletion of NL3, we aspirated the cytosol of individual MSNs in both the ventral and dorsal striatum (Figure 3O), and measured by quantitative RT-PCR the mRNA levels of different neuroligin isoforms as well as of markers that differentiate D1- and D2-MSNs (Heiman et al., 2008). Robust differences in these cell type-specific markers confirmed successful isolation of single MSNs (Figure 3P). In the NAc, NL3 mRNA levels were significantly higher in D1-MSNs than in D2-MSNs, with no differences in NL1 or NL2 levels (Figure 3Q). In the dorsal striatum, however, the differential NL3 expression that we observed in the NAc was not apparent, and NL3 was expressed at similarly low levels in both MSN subtypes (Figures 3R and S4).

To determine the behavioral consequences of spatially restricted NL3 deletions from either the dorsal striatum or the NAc, we used NL3-cKO mice and performed *in vivo* stereotactic injections of adeno-associated viruses (AAVs) that express Cre recombinase fused with GFP under control of the synapsin promoter (Figure 4A). A second virus encoding a catalytically inactive version of Cre recombinase (ΔCre) was used as a control. Widespread deletion of NL3 in the dorsal striatum had no effect on either rotarod performance or open field activity (Figures 4B-4G). Deletion of NL3 in the NAc, however, significantly enhanced rotarod learning and increased open field activity (Figures 4H-4M). While consistent with the high level of NL3 expression in D1-MSNs of the NAc, these results are somewhat unexpected because the NAc is commonly associated with reward-related behaviors, rather than motor function (Balleine and O'Doherty, 2010; Graybiel, 2008; Yin and Knowlton, 2006). Viral expression of Cre in the NAc had no effect on the enhanced rotarod learning of NL3-R451C mutant mice (Figures S3E-S3G), suggesting that the R451C mutation (which decreases NL3 protein levels) was already causing a loss of NL3 function in this circuit.

Although viral injections allow NL3 deletions in a specific striatal subregion, they do not restrict this deletion to specific cell types. In order to definitively address the role of D1-MSNs in the NAc, we implemented a “rescue” strategy to restore NL3 function in this subpopulation of neurons. We constructed an AAV that contains NL3- and mVenus-expression cassettes orientated as a double-inverse open reading frame (DIO; Figure 5A). Injection of this AAV into the NAc of NL3-cKO mice carrying D1-Cre restores NL3 function only in D1-MSNs at the site of injection (see Figure 5A, inset). This manipulation

abolished the phenotype caused by conditional NL3 deletion in D1-MSNs, as the behavior of these mice was identical to a control group lacking D1-Cre (Figures 5B-5G). Together, these experiments identify D1-MSNs in the NAc as a critical node in the molecular circuitry mediating the behavioral consequences of the NL3 deletion.

Bidirectional Control of Behavior by Subtypes of NAc MSNs

The preceding results are surprising in light of previous literature implicating the dorsal striatum in rotarod learning (Costa et al., 2004; Yin et al., 2009). We therefore sought to independently validate the relative contributions of D1- and D2-MSNs in the NAc and dorsal striatum to rotarod performance and open field activity. To this end, we developed an AAV that expresses an engineered Kir2.1 K^+-channel subunit in a Cre-dependent fashion (DIO-Kir; Lin et al., 2010). We injected this virus into D1-Cre and A2a-Cre mice (Figure 6A). As expected, infected MSNs fired fewer spikes in response to depolarizing current injections, and exhibited a reduced input resistance and an increased action potential firing threshold (Figures 6B and 6C). This virus was used to investigate the behavioral consequences of downregulating the activity of specific MSN subtypes in the NAc or dorsal striatum.

Expression of DIO-Kir in the NAc of D1-Cre mice did not affect performance on early trials of the accelerating rotarod, but significantly reduced performance late in training (Figures 6D-6F). The opposite effect was observed following injection into the NAc of A2a-Cre mice (which express Cre in D2-MSNs), with enhanced performance late in training (Figures 6H-6J). Open field activity in these same mice was also altered in a bidirectional fashion, with D1-Cre and A2a-Cre exhibiting decreases and increases in activity, respectively (Figures 6G and 6K).

Injection of DIO-Kir into the dorsal striatum produced a very different phenotypic pattern. In D1-Cre mice, it caused a dramatic impairment in rotarod performance that was evident from the first trial and persisted throughout testing, indicating reduced motor coordination (Figures 6L-6N). Analogous experiments with A2a-Cre mice produced no phenotype (Figures 6P-6R), and open field activity was not altered by any manipulation of the dorsal striatum (Figures 6O and 6S).

To compare the impact of manipulating different cell types in different striatal subregions, we normalized the performance of each experimental group to their wild-type littermate controls for the first and last trials of rotarod testing and for open field activity (Figures 6T-6V). These results demonstrated that the balance between activation of D1- and D2-MSNs in the NAc dynamically regulates behavior in the same tasks that are altered by NL3 deletion, while MSNs in the dorsal striatum play a different behavioral role. The data also show that behavioral regulation of open field activity and rotarod performance can be dissociated at the circuit level, as already indicated by the analysis of the cerebellar function of NL3 (Figure 2).

NL3 Deletion Impairs Synaptic Inhibition of D1-MSNs in the NAc

To test the hypothesis that deletion of NL3 alters synaptic transmission onto D1-MSNs of the NAc, we performed whole-cell voltage-clamp recordings in acute slices from NL3-KO

mice. These mice were crossed with a D1-tomato reporter line, permitting targeted recordings from red D1-MSNs and non-fluorescent D2-MSNs. We first investigated excitatory synaptic function in both MSN subtypes by recording spontaneous miniature excitatory postsynaptic currents (mEPSCs), but detected no changes in D1- or D2-MSNs in NL3-KO mice (Figures 7A and 7B). There were also no substantial changes in the paired-pulse ratio of evoked EPSCs, and the complement and subunit composition of synaptic AMPA and NMDA receptors appeared normal in both MSN subtypes (Figure S5).

Alterations in the function of metabotropic glutamate receptors (mGluRs), particularly mGluR-dependent long-term depression (LTD), have been reported in several ASD mouse models (Auerbach et al., 2011; Baudouin et al., 2012). Bath application of a group I mGluR agonist, DHPG, caused a transient depression of EPSC amplitude in D1-MSNs that was similar in wild-type and NL3-KO mice (Figure 7C). DHPG caused a long-lasting depression of the EPSC amplitude that was also indistinguishable between wild-type and NL3-KO mice (Figure 7D). These results indicate that the function of group I mGluRs in MSNs of the NAc is not grossly altered by deletion of NL3.

A major component of mGluR-dependent LTD in the NAc involves postsynaptic release of endocannabinoids and activation of presynaptic CB1 receptors, leading to reduced probability of glutamate release (Grueter et al., 2010). In our experiments, this reduction in glutamate release manifested as an increase in paired-pulse ratio, with similar magnitudes in both wild-type (29 + 9%) and NL3-KO mice (20 + 9%). Thus, the NL3-KO mutation does not affect the molecular machinery required for synthesis and detection of endocannabinoids at NAc excitatory synapses.

We next assessed inhibitory synaptic function in NL3-KO mice, and recorded miniature inhibitory postsynaptic synaptic currents (mIPSCs) in the NAc. Strikingly, we found that in D1-MSNs, the mIPSC frequency was reduced by ∼50% in NL3-KO and NL3-R451C mutant mice, whereas the mIPSC amplitude was unchanged (Figures. 7E and S6A), indicating both ASD-associated NL3 mutations have a common synaptic effect in this circuit. In D2-MSNs, the NL3-KO mutation produced no significant change in mIPSC frequency or amplitude (Figure 7F). Thus, loss of NL3 causes a cell type-specific reduction of synaptic inhibition onto D1-MSNs of the NAc – the same subpopulation of neurons responsible for the behavioral impact of the NL3 deletion. Neither NL3 mutation affected mIPSC frequency or amplitude in D1-MSNs of the dorsal striatum (Figures S6B-S6C), consistent with the low expression of NL3 in these cells (Figure S4D).

Decreases in mIPSC frequency can be caused by a lower probability of GABA release, but we detected no significant changes in the paired-pulse ratio of evoked IPSCs or short-term plasticity (Figures S6D-S6E). Loss of NL3 in the hippocampus has been reported to disrupt the regulation of GABA release by tonic endocannabinoid signaling (Foldy et al., 2013). In D1-MSNs of the NAc, we found no evidence for tonic endocannabinoid regulation of GABA release, as bath application of a CB1 receptor antagonist (AM251) did not alter the evoked IPSC amplitude in either genotype (Figure 7G). To assess the presence and functional integrity of presynaptic CB1 receptors, we applied a CB1 receptor agonist (WIN55, 212), which caused a similar substantial reduction of evoked IPSC amplitudes in

WT and NL3-KO mice (Figure 7H). These results suggest that endocannabinoid signaling at inhibitory synapses onto D1-MSNs is not affected by deletion of NL3. We also failed to detect changes in the synaptic concentration of released GABA (Figure S6F), or the number of perisomatic inhibitory synapses on D1-MSNs (Figures S6G-S6I).

The fact that the NL3-KO mutation decreased inhibitory synaptic currents in D1-MSNs of the NAc, coupled with the apparently normal function of excitatory synapses, implies that loss of NL3 shifts the balance between synaptic excitation and inhibition in this cell type. To directly address this possibility, we experimentally measured the ratio between GABA receptor-mediated inhibition and AMPA receptor-mediated excitation (Figure 7I). After recording an evoked AMPA receptor current at a holding potential of -40 mV, we depolarized cells to 0 mV and blocked AMPA receptors with NBQX, leaving a residual current mediated by monosynaptic inhibition through GABA receptors. The ratio of peak GABA receptor- to peak AMPA receptor-mediated currents (i.e., the inhibition/excitation ratio) was significantly reduced in D1-MSNs but not D2-MSNs from NL3-KO mice (Figures 7J and 7K). Moreover, when we normalized the disinhibition of D1-MSNs by targeted viral expression of DIO-Kir, we abolished the behavioral phenotypes caused by deletion of NL3 (Figures S7A-S7G). Together, these results reveal a cell type-specific imbalance of synaptic excitation and inhibition in D1-MSNs of the NAc caused by NL3 mutations associated with ASD (Figures S7H-S7K).

Discussion

Establishing causality between a genetic mutation, synaptic changes, circuit dysfunction, and abnormal behavior is one of the greatest contributions mouse models can potentially make to understanding neuropsychiatric diseases. Establishing such causality, however, has been difficult. To forge these connections, we examined the specific synaptic cause of a robust behavioral phenotype that is commonly shared by multiple mouse models of ASDs, namely the enhanced formation of a repetitive motor routine as measured on the accelerating rotarod (Table S1). We used a “top-down” approach by first localizing the brain region, then the cell type, and finally the synaptic connection affected by different mutations of NL3, and provided evidence that this particular synaptic change accounts for the overall behavioral phenotype observed. Specifically, we found that the enhanced formation of a repetitive motor routine is caused by loss-of-function of NL3 in D1-MSNs but not D2-MSNs of the NAc but not the dorsal striatum, and that the NL3 loss-of-function acts by producing a selective reduction of synaptic inhibition onto NAc D1-MSNs. To the best of our knowledge, this is the first localization of an ASD-related behavioral change to a particular type of synapse in a specific neuronal cell type and a defined brain region.

Several aspects of our results are surprising. First, the enhanced formation of repetitive motor routines, observed in both NL3-KO and R451C mutant mice, did not appear to involve either the dorsal striatum or the cerebellum. Although previous studies link synaptic dysfunction in these brain regions to ASD pathophysiology (Baudouin et al., 2012; Peca et al., 2011), we found no behavioral connection between these brain regions and the rotarod phenotype we observed in NL3 mutant mice. Instead, our data show that loss of NL3 in D1-MSNs of the NAc is both necessary and sufficient to enhance repetitive motor routines.

While deletion of NL3 in cerebellar Purkinje cells (using L7-Cre) had no effect on rotarod performance, it did cause hyperactivity in the open field test, another behavioral phenotype shared by NL3-KO and R451C mutant mice. Rotarod performance was also unaffected by deletion of NL3 in all neurons that express parvalbumin (using PV-Cre), but this manipulation unexpectedly caused a *decrease* in open field activity – opposite to the phenotype of NL3-KO mice or the deletion of NL3 in only Purkinje cells. These findings demonstrate that deletion of a single molecule in different types of neurons can produce heterogeneous and even opposite effects on behavioral output. This may help to explain the diverse clinical presentations of individual patients carrying the same genetic mutation, because individual differences in other genetic and environmental factors could render various circuits differentially vulnerable to the impact of such mutations.

A second surprising aspect of our results is that our molecular manipulations of NL3 resulted in the same phenotypes independent of whether expression was constitutively blocked throughout development, or conditionally deleted in adult animals. This unexpected observation suggests that neuroligins perform a continuous synaptic function throughout life, and not just during development. This observation adds to a growing literature indicating that mouse models of neurodevelopmental disorders remain amenable to interventions performed in adulthood (Baudouin et al., 2012; Penagarikano et al., 2011; Zoghbi and Bear, 2012), reinforcing hopes that clinical treatment of these disorders in adult patients could still be effective.

Finally, the role of NL3 in the NAc but not the dorsal striatum is also surprising, given previous studies implicating the dorsal striatum in rotarod performance (Costa et al., 2004; Yin et al., 2009). However, other studies linking striatal circuitry to rotarod learning used manipulations that affect both dorsal and ventral striatum (Dang et al., 2006). While the relatively enriched expression of NL3 in D1-MSNs of the NAc biases its contribution to this brain region and cell type, our experiments with DIO-Kir show that both the NAc and the dorsal striatum normally shape rotarod performance. D1-MSNs in the dorsal striatum were important for overall motor coordination, whereas D1- and D2-MSNs in the NAc contributed to rotarod learning and to open field activity in a bidirectional fashion.

These data support the theory that different striatal subregions interact dynamically over the normal course of learning (Balleine and O'Doherty, 2010; Graybiel, 2008; Yin and Knowlton, 2006), with the NAc gating the transition to dorsal striatal control of behavior (Belin and Everitt, 2008; Haber et al., 2000). One intriguing possibility is that deletion of NL3 accelerates this transition from ventral to dorsal striatal control, a process that may also be facilitated by mutations directly affecting the dorsal striatum (Peca et al., 2011). This may promote the acquisition of repetitive motor routines as well as rigid and inflexible habits (Balleine and O'Doherty, 2010; Graybiel, 2008; Yin and Knowlton, 2006). While our results do not bear directly on the cognitive process of habit formation, they do implicate overlapping striatal circuitry, making this a fascinating topic for future research. Our results also highlight the integrative function of the NAc in processing sensory and limbic information to generate adaptive motor outputs (Groenewegen et al., 1996). Coupled with evidence implicating the NAc in social behavior and reward processing (Trezza et al., 2011),

our data suggest that synaptic dysfunction in the NAc may contribute to a wide array of ASD symptoms.

Our slice physiology experiments revealed a remarkable degree of specificity in the synaptic consequences of deleting NL3. We failed to detect any change in either excitatory or inhibitory synaptic function in D2-MSNs, including normal mGluR-LTD at excitatory synapses – a form of synaptic plasticity altered in cerebellar Purkinje cells of NL3-KO mice (Baudouin et al., 2012). Our results thus indicate that dysregulation of mGluR-dependent LTD is not an inevitable synaptic consequence of the NL3 deletion, and does not account for the behavioral abnormality we have identified.

Excitatory synaptic function in D1-MSNs of the NAc also appeared normal, but we identified a robust (∼50%) reduction of inhibitory synaptic currents. The cell type- and subregion-specificity of this synaptic deficit is consistent with high expression of NL3 in D1-MSNs of the NAc, as well as the behavioral consequences of conditional NL3 deletion from these particular cells. The loss of synaptic inhibition was not mediated by altered endocannabinoid signaling (Foldy et al., 2013), but led to a shift in the ratio between synaptic inhibition and excitation, which we directly quantified in single neurons. The disinhibition of D1-MSNs caused by deletion of NL3 would tilt the balance between activation of MSN subtypes in the NAc. Our experiments using DIO-Kir demonstrated that this imbalance can plausibly explain the behavioral phenotypes caused by the NL3-KO and R451C mutations (Figure S7). These results reinforce a general scheme of striatal circuit function in which D1-MSNs of the direct pathway promote the execution and repetition of specific motor sequences, while D2-MSNs of the indirect pathway inhibit competing motor sequences (Gerfen and Surmeier, 2011; Kreitzer and Malenka, 2008).

The balance between synaptic excitation and inhibition is thought to be a key factor governing neural circuit function, and may be disrupted by a number of ASD-associated genetic mutations (Bateup et al., 2013; Etherton et al., 2009; Tabuchi et al., 2007). However, the nature of this disruption depends on the exact mutation, cell type, and synapse under consideration, indicating that ‘excitatory/inhibitory balance’ must be interpreted in the context of specific cells and circuits to have disease relevance. Indeed, the NL3-KO and R451C mutations have previously been shown to enhance synaptic inhibition in the hippocampus (Foldy et al., 2013) and cortex (Tabuchi et al., 2007). The opposite result we observe in the NAc can likely be explained by a unique complement of other pre- and post-synaptic cell adhesion molecules expressed at these different synaptic connections, which work in concert to dictate synaptic properties.

In this respect, our results highlight the enormous diversity of synaptic phenotypes emerging from ongoing descriptions of ASD mouse models. Different ASD-associated mutations can cause opposite changes in some synaptic parameters (Auerbach et al., 2011), while a single mutation can have distinct synaptic effects in different brain regions (present results, as well as Etherton et al., 2011), or even at different synapses on the same type of neuron (Foldy et al., 2013). This extraordinary complexity highlights a growing need to pinpoint the specific brain regions, cell types, and synaptic connections most relevant to the behavioral impact of ASD-associated mutations. We believe that deciphering the molecular circuitry behind these

mutations could lead to unifying hypotheses regarding the diverse genetic causes of ASD. Using this knowledge to guide investigations of synaptic and cellular mechanisms should lead to the rational design of more specific and efficacious therapeutic interventions.

Experimental Procedures

Animals

NL3-cKO mice were produced using standard procedures (Figure S2). All other mice were described previously (see Supplemental Methods for details). All analyses were performed on male littermate mice (at least 4 weeks old for physiology and *in vivo* stereotactic injections, and at least 6 weeks old mice for behavioral studies) after extensive backcrossing to C57Bl/6J except when noted. All analyses were performed on mice whose genotype was unknown to the experimenter. All procedures conformed to National Institutes of Health *Guidelines for the Care and Use of Laboratory Animals* and were approved by the Stanford University Administrative Panel on Laboratory Animal Care.

Behavioral Assays

Rotarod testing consisted of three trials per day over the course of 4 days. Each trial ended when a mouse fell off, made one complete backwards revolution while hanging on, or reached 300 s (Etherton et al., 2009). Digital videos of WT and NL3-KO mice on the rotarod were recorded from behind to manually track the location of rear paws. Open field activity tests (Grueter et al., 2010) and force plate actometer assays (Fowler et al., 2001) were performed using standard approaches.

Molecular Methods

Quantitative RT-PCR and quantitative immunoblotting experiments were performed on brain tissues derived from the same mice as described (Tabuchi et al., 2007; Aoto et al., 2013). For single-cell transcriptional analyses, individual MSNs from D1-tdTomato BAC transgenic mice were aspirated under DIC optics (see Supplemental Methods for details).

Stereotactic Injections

Stereotactic injections of AAVs were performed as described (Aoto et al., 2013). Fluorescent protein tags expressed by each viral construct were used to confirm efficiency and localization of AAV infection.

Electrophysiology

Parasagittal slices (250 μm) containing the NAc were prepared from wild-type and NL3-KO mice carrying the D1-tomato reporter gene, permitting identification of red D1-MSNs and non-fluorescent D2-MSNs. Whole-cell voltage- and current-clamp recordings were performed at 30 °C using standard procedures (Grueter et al., 2010), with pharmacological isolation of EPSCs and IPSCs as described in the Supplemental Methods.

Immunohistochemistry

Vibratome sections from perfusion-fixed mouse brains were stained with antibodies for immunofluorescence imaging on a Zeiss confocal microscope and analyzed in Image-J. The number of VGAT positive puncta immediately adjacent to tomato-positive neurons were counted by hand.

Data Analysis

All comparisons relate test to control data from littermate animals collected during the same time period, and were analyzed statistically using ANOVA with a Type I error rate $\alpha = 0.05$ (two-tailed). When ANOVA results are presented in figures, significant effects are highlighted; non-significant comparisons are not identified.

Supplementary Material

Refer to Web version on PubMed Central for supplementary material.

Acknowledgments

We thank A. Darvishzadeh, A. Afjei, G. Sun, S. Ghosh, and N. Huang for technical assistance, C. Földy for advice, and all Malenka and Südhof lab members for helpful discussions. This work was supported by grants from the NIMH (P50 MH086403 to R.C.M. and T.C.S., K99 MH099243 to M.V.F., and F32 MH096491 to P.E.R.); initial stages were also supported by the Simons Foundation (to R.C.M. and T.C.S.).

References

Akil H, Brenner S, Kandel E, Kendler KS, King MC, Scolnick E, Watson JD, Zoghbi HY. Medicine. The future of psychiatric research: genomes and neural circuits. Science. 2010; 327:1580–1581. [PubMed: 20339051]

Aoto J, Martinelli DC, Malenka RC, Tabuchi K, Südhof TC. Presynaptic Neurexin-3 Alternative Splicing Trans-Synaptically Controls Postsynaptic AMPA-Receptor Trafficking. Cell. 2013; 154:75–88. [PubMed: 23827676]

Auerbach BD, Osterweil EK, Bear MF. Mutations causing syndromic autism define an axis of synaptic pathophysiology. Nature. 2011; 480:63–68. [PubMed: 22113615]

Balleine BW, O'Doherty JP. Human and rodent homologies in action control: corticostriatal determinants of goal-directed and habitual action. Neuropsychopharmacology. 2010; 35:48–69. [PubMed: 19776734]

Bateup HS, Johnson CA, Denefrio CL, Saulnier JL, Kornacker K, Sabatini BL. Excitatory/inhibitory synaptic imbalance leads to hippocampal hyperexcitability in mouse models of tuberous sclerosis. Neuron. 2013; 78:510–522. [PubMed: 23664616]

Baudouin SJ, Gaudias J, Gerharz S, Hatstatt L, Zhou K, Punnakkal P, Tanaka KF, Spooren W, Hen R, De Zeeuw CI, et al. Shared synaptic pathophysiology in syndromic and nonsyndromic rodent models of autism. Science. 2012; 338:128–132. [PubMed: 22983708]

Belin D, Everitt BJ. Cocaine seeking habits depend upon dopamine-dependent serial connectivity linking the ventral with the dorsal striatum. Neuron. 2008; 57:432–441. [PubMed: 18255035]

Chadman KK, Gong S, Scattoni ML, Boltuck SE, Gandhy SU, Heintz N, Crawley JN. Minimal aberrant behavioral phenotypes of neuroligin-3 R451C knockin mice. Autism Res. 2008; 1:147–158. [PubMed: 19360662]

Comoletti D, De Jaco A, Jennings LL, Flynn RE, Gaietta G, Tsigelny I, Ellisman MH, Taylor P. The Arg451Cys-neuroligin-3 mutation associated with autism reveals a defect in protein processing. J Neurosci. 2004; 24:4889–4893. [PubMed: 15152050]

Costa RM, Cohen D, Nicolelis MA. Differential corticostriatal plasticity during fast and slow motor skill learning in mice. Curr Biol. 2004; 14:1124–1134. [PubMed: 15242609]

Dang MT, Yokoi F, Yin HH, Lovinger DM, Wang Y, Li Y. Disrupted motor learning and long-term synaptic plasticity in mice lacking NMDAR1 in the striatum. Proc Natl Acad Sci U S A. 2006; 103:15254–15259. [PubMed: 17015831]

Di Martino A, Kelly C, Grzadzinski R, Zuo XN, Mennes M, Mairena MA, Lord C, Castellanos FX, Milham MP. Aberrant striatal functional connectivity in children with autism. Biol Psychiatry. 2011; 69:847–856. [PubMed: 21195388]

Durieux PF, Bearzatto B, Guiducci S, Buch T, Waisman A, Zoli M, Schiffmann SN, de Kerchove d'Exaerde A. D2R striatopallidal neurons inhibit both locomotor and drug reward processes. Nat Neurosci. 2009; 12:393–395. [PubMed: 19270687]

Etherton M, Foldy C, Sharma M, Tabuchi K, Liu X, Shamloo M, Malenka RC, Sudhof TC. Autism-linked neuroligin-3 R451C mutation differentially alters hippocampal and cortical synaptic function. Proc Natl Acad Sci U S A. 2011; 108:13764–13769. [PubMed: 21808020]

Etherton MR, Blaiss CA, Powell CM, Sudhof TC. Mouse neurexin-1α deletion causes correlated electrophysiological and behavioral changes consistent with cognitive impairments. Proc Natl Acad Sci U S A. 2009; 106:17998–18003. [PubMed: 19822762]

Fishell G, Rudy B. Mechanisms of inhibition within the telencephalon: “where the wild things are”. Annu Rev Neurosci. 2011; 34:535–567. [PubMed: 21469958]

Foldy C, Malenka RC, Sudhof TC. Autism-associated neuroligin-3 mutations commonly disrupt tonic endocannabinoid signaling. Neuron. 2013; 78:498–509. [PubMed: 23583622]

Fowler SC, Birkestrand BR, Chen R, Moss SJ, Vorontsova E, Wang G, Zarcone TJ. A force-plate actometer for quantitating rodent behaviors: illustrative data on locomotion, rotation, spatial patterning, stereotypies, and tremor. Journal of neuroscience methods. 2001; 107:107–124. [PubMed: 11389948]

Gerfen CR, Surmeier DJ. Modulation of striatal projection systems by dopamine. Annu Rev Neurosci. 2011; 34:441–466. [PubMed: 21469956]

Graybiel AM. Habits, rituals, and the evaluative brain. Annu Rev Neurosci. 2008; 31:359–387. [PubMed: 18558860]

Groenewegen HJ, Wright CI, Beijer AV. The nucleus accumbens: gateway for limbic structures to reach the motor system? Prog Brain Res. 1996; 107:485–511. [PubMed: 8782538]

Grueter BA, Brasnjo G, Malenka RC. Postsynaptic TRPV1 triggers cell type-specific long-term depression in the nucleus accumbens. Nat Neurosci. 2010; 13:1519–1525. [PubMed: 21076424]

Haber SN, Fudge JL, McFarland NR. Striatonigrostriatal pathways in primates form an ascending spiral from the shell to the dorsolateral striatum. J Neurosci. 2000; 20:2369–2382. [PubMed: 10704511]

Heiman M, Schaefer A, Gong S, Peterson JD, Day M, Ramsey KE, Suarez-Farinas M, Schwarz C, Stephan DA, Surmeier DJ, et al. A translational profiling approach for the molecular characterization of CNS cell types. Cell. 2008; 135:738–748. [PubMed: 19013281]

Hikosaka O, Nakamura K, Sakai K, Nakahara H. Central mechanisms of motor skill learning. Curr Opin Neurobiol. 2002; 12:217–222. [PubMed: 12015240]

Hollander E, Anagnostou E, Chaplin W, Esposito K, Haznedar MM, Licalzi E, Wasserman S, Soorya L, Buchsbaum M. Striatal volume on magnetic resonance imaging and repetitive behaviors in autism. Biol Psychiatry. 2005; 58:226–232. [PubMed: 15939406]

Jamain S, Quach H, Betancur C, Rastam M, Colineaux C, Gillberg IC, Soderstrom H, Giros B, Leboyer M, Gillberg C, et al. Mutations of the X-linked genes encoding neuroligins NLGN3 and NLGN4 are associated with autism. Nat Genet. 2003; 34:27–29. [PubMed: 12669065]

Jamain S, Radyushkin K, Hammerschmidt K, Granon S, Boretius S, Varoqueaux F, Ramanantsoa N, Gallego J, Ronnenberg A, Winter D, et al. Reduced social interaction and ultrasonic communication in a mouse model of monogenic heritable autism. Proc Natl Acad Sci U S A. 2008; 105:1710–1715. [PubMed: 18227507]

Kreitzer AC, Malenka RC. Striatal plasticity and basal ganglia circuit function. Neuron. 2008; 60:543–554. [PubMed: 19038213]

Langen M, Schnack HG, Nederveen H, Bos D, Lahuis BE, de Jonge MV, van Engeland H, Durston S. Changes in the developmental trajectories of striatum in autism. Biol Psychiatry. 2009; 66:327–333. [PubMed: 19423078]

Levy D, Ronemus M, Yamrom B, Lee YH, Leotta A, Kendall J, Marks S, Lakshmi B, Pai D, Ye K, et al. Rare de novo and transmitted copy-number variation in autistic spectrum disorders. Neuron. 2011; 70:886–897. [PubMed: 21658582]

Lin CW, Sim S, Ainsworth A, Okada M, Kelsch W, Lois C. Genetically increased cell-intrinsic excitability enhances neuronal integration into adult brain circuits. Neuron. 2010; 65:32–39. [PubMed: 20152111]

Nestler EJ, Hyman SE. Animal models of neuropsychiatric disorders. Nat Neurosci. 2010; 13:1161–1169. [PubMed: 20877280]

Peca J, Feliciano C, Ting JT, Wang W, Wells MF, Venkatraman TN, Lascola CD, Fu Z, Feng G. Shank3 mutant mice display autistic-like behaviours and striatal dysfunction. Nature. 2011; 472:437–442. [PubMed: 21423165]

Penagarikano O, Abrahams BS, Herman EI, Winden KD, Gdalyahu A, Dong H, Sonnenblick LI, Gruver R, Almajano J, Bragin A, et al. Absence of CNTNAP2 leads to epilepsy, neuronal migration abnormalities, and core autism-related deficits. Cell. 2011; 147:235–246. [PubMed: 21962519]

Presti MF, Watson CJ, Kennedy RT, Yang M, Lewis MH. Behavior-related alterations of striatal neurochemistry in a mouse model of stereotyped movement disorder. Pharmacology, biochemistry, and behavior. 2004; 77:501–507.

Radyushkin K, Hammerschmidt K, Boretius S, Varoqueaux F, El-Kordi A, Ronnenberg A, Winter D, Frahm J, Fischer J, Brose N, et al. Neuroligin-3-deficient mice: model of a monogenic heritable form of autism with an olfactory deficit. Genes Brain Behav. 2009; 8:416–425. [PubMed: 19243448]

Sanders SJ, Ercan-Sencicek AG, Hus V, Luo R, Murtha MT, Moreno-De-Luca D, Chu SH, Moreau MP, Gupta AR, Thomson SA, et al. Multiple recurrent de novo CNVs, including duplications of the 7q11.23 Williams syndrome region, are strongly associated with autism. Neuron. 2011; 70:863–885. [PubMed: 21658581]

Sudhof TC. Neuroligins and neurexins link synaptic function to cognitive disease. Nature. 2008; 455:903–911. [PubMed: 18923512]

Tabuchi K, Blundell J, Etherton MR, Hammer RE, Liu X, Powell CM, Sudhof TC. A neuroligin-3 mutation implicated in autism increases inhibitory synaptic transmission in mice. Science. 2007; 318:71–76. [PubMed: 17823315]

Trezza V, Damsteegt R, Achterberg EJ, Vanderschuren LJ. Nucleus accumbens mu-opioid receptors mediate social reward. J Neurosci. 2011; 31:6362–6370. [PubMed: 21525276]

Yin HH, Knowlton BJ. The role of the basal ganglia in habit formation. Nat Rev Neurosci. 2006; 7:464–476. [PubMed: 16715055]

Yin HH, Mulcare SP, Hilario MR, Clouse E, Holloway T, Davis MI, Hansson AC, Lovinger DM, Costa RM. Dynamic reorganization of striatal circuits during the acquisition and consolidation of a skill. Nat Neurosci. 2009; 12:333–341. [PubMed: 19198605]

Zoghbi HY, Bear MF. Synaptic dysfunction in neurodevelopmental disorders associated with autism and intellectual disabilities. Cold Spring Harb Perspect Biol. 2012; 4

Highlights

- Neuroligin-3 mutations commonly enhance repetitive motor routines in mice
- Repetitive behavior requires neuroligin-3 function in the nucleus accumbens
- Neuroligin-3 is selectively essential in D1 -dopamine receptor containing neurons
- Neuroligin-3 deletion impairs synaptic inhibition on striatal medium spiny neurons

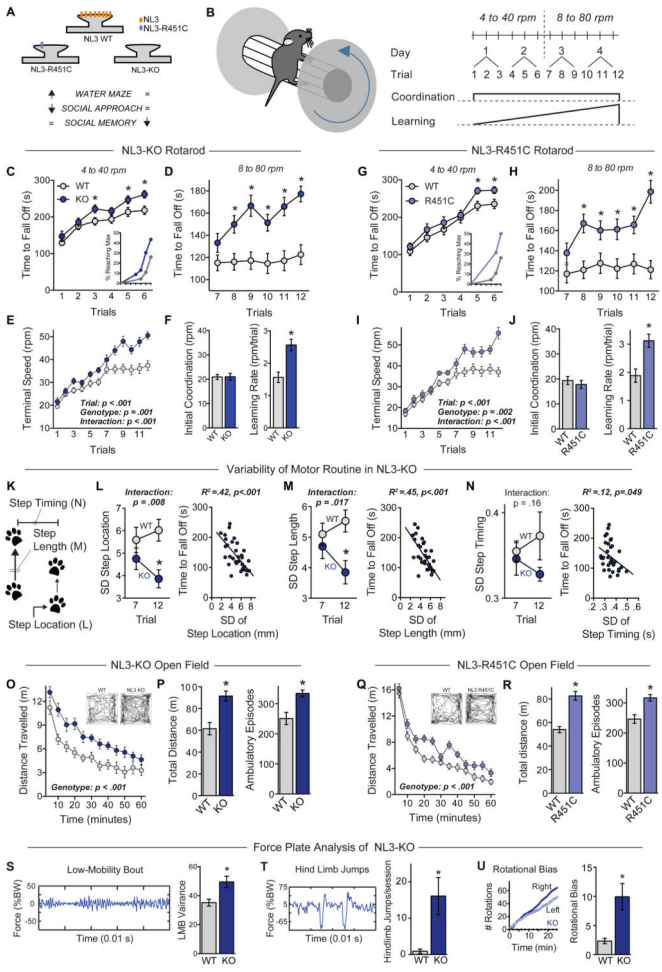

Figure 1. ASD-associated NL3 mutations enhance repetitive and stereotyped behaviors

(A) Summary of behavioral heterogeneity in ASD mouse models produced by NL3 mutations.

(B) Illustration of a mouse on a rotarod (left), and diagram of the rotarod testing protocol (right). The effects of motor coordination and learning are illustrated below the protocol.

(C-F) Performance of littermate wild-type (WT, n=22) and NL3-KO mice (n=23) on the accelerating rotarod. Time to fall off is presented at *4 to 40 rpm* (C) and *8 to 80 rpm* (D); the terminal speed of rotation (E) was used to calculate initial coordination and learning rate (F). Inset in C shows percentage of mice reaching maximum performance time (300 s) plotted as a function of trial.

(G-J) Same as C-F, but comparing WT (n=19) and NL3-R451C mutant mice (n=16).

(K-N) Quantitative video analysis of acquisition rates of repetitive motor routines during rotarod training (n=8 WT and 9 NL3-KO mice). K illustrates the analyzed parameters: step location, step length, and step timing. L-N depicts the standard deviation (SD) of step location (L), step length (M), and time between steps (N) calculated on trials 7 and 12 during rotarod training to measure variability in the motor routine (left panels), as well as the correlation with time to fall off the rotarod (right panels).

(O & P) Behavior of WT and NL3-KO mice in an open field test, showing time course of activity across the entire session (O), as well as total distance travelled and the number of ambulatory episodes (P). Insets depict movement path of individual mice 10-20 min after the test begins.

(Q & R) Open field activity for WT and NL3-R451C mice.

(S-U) Analysis of stereotyped behaviors by measurements of the force plate variance as percentage of body weight (%BW) during low-mobility bouts (LMB, S), hind limb jumps (T), and rotational bias during locomotion (U) in WT (n=10) and NL3-KO mice (n=12). Data are means + SEM; *significant difference between groups (ANOVA). Also see Table S1 and Figure S1.

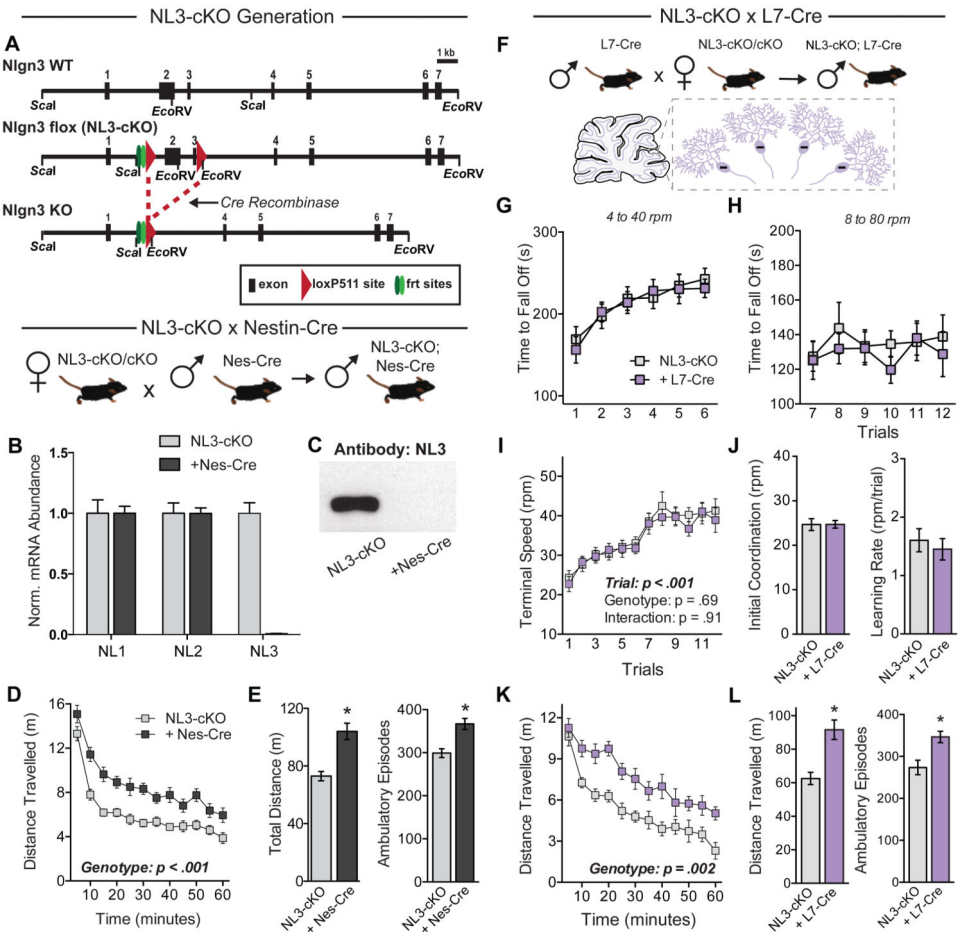

Figure 2. Conditional removal of NL3 in cerebellar Purkinje cells does not affect rotarod performance but causes hyperactivity

(A) Strategy for generation of NL3 conditional knockout (NL3-cKO) mice. Top, structure of the 5′ end of the wild-type mouse *Nlgn3* gene; middle, structure of the cKO *Nlgn3* gene in which loxP511 sites flank exons 2 and 3 (“flox”); and bottom, structure of the KO gene after Cre-recombinase mediated deletion of exons 2 and 3.

(B) Levels of NL1, NL2, and NL3 mRNAs in brains of NL3-cKO mice without (n=4) or with nestin-Cre (Nes-Cre, n=4).

(C) NL3 immunoblot of whole brain protein from NL3-cKO mice with and without Nes-Cre.

(D & E) Analysis of littermate NL3-cKO mice without (n=16) or with Nes-Cre (n=16) in the open field test. Data show the time course of activity across the entire session (D) as well as the total distance traveled and the number of ambulatory episodes (E).

(F) Illustration of genetic cross to selectively delete NL3 from cerebellar Purkinje cells.

(G-J) Rotarod performance of NL3-cKO mice without (n=11) or with L7-cre expression in cerebellar Purkinje cells (n=11). Time to fall off is presented at *4 to 40 rpm* (G) and *8 to 80 rpm* (H); the terminal speed of rotation (I) was used to calculate initial coordination and learning rate (J).

(K & L) Behavior in a test of open field activity after Purkinje cell deletion of NL3.

Data are means ± SEM; *significant difference between groups (ANOVA). Also see Figure S2.

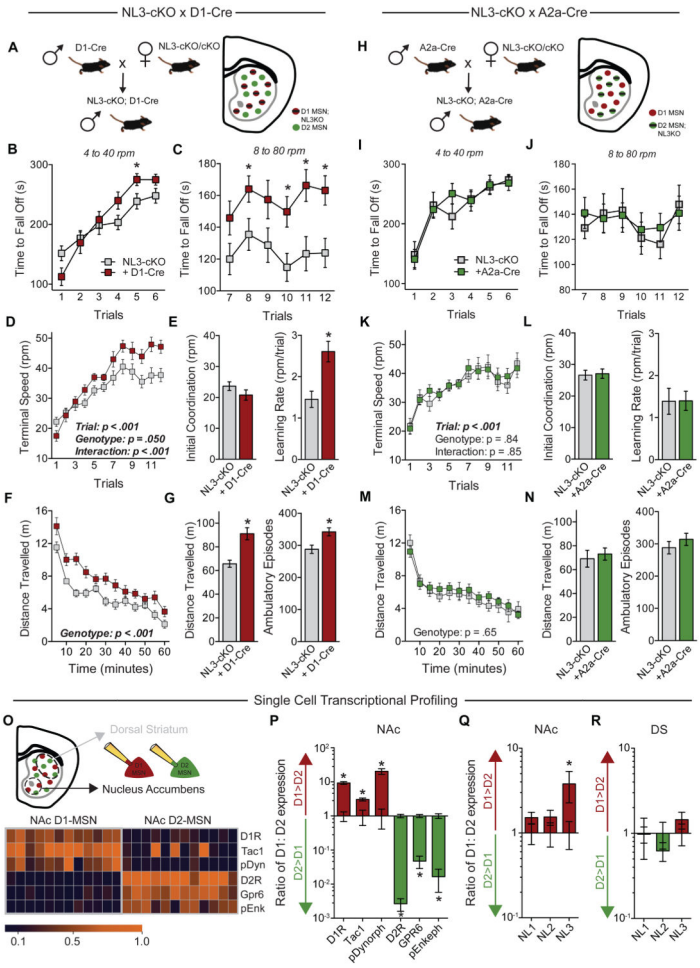

Figure 3. Enhanced acquisition of repetitive motor routines requires NL3 expression in striatal D1-MSNs but not D2-MSNs

(A) Illustration of genetic cross used to specifically delete NL3 from D1-MSNs.

(B-E) Rotarod performance of NL3-cKO mice without (n=16) and with D1-Cre (n=12). Time to fall off is presented at *4 to 40 rpm* (B) and *8 to 80 rpm* (C); the terminal speed of rotation (D) was used to calculate initial coordination and learning rate (E).

(F & G) Behavior of the same mice in a test of open field activity, showing time course of activity across the entire session (F) as well as total distance travelled and number of ambulatory episodes (G).

(H-N) Behavior of NL3-cKO mice without (n=8) and with A2a-Cre (n=10), which directs Cre expression exclusively to D2-MSNs.

(O) Illustration of cytosol aspiration from individual D1- and D2-MSNs of the NAc (top), and quantitative RT-PCR results from individual cells showing mRNA expression of cell type-specific markers (bottom).

(P-R) Relative mRNA expression quantified as the ratio between D1- and D2-MSNs, showing cell type-specific markers in the NAc (P) as well as neuroligins in the NAc (Q) and dorsal striatum (R).

Data are means ± SEM; *significant difference between groups (ANOVA). Also see Figures S3 & S4.

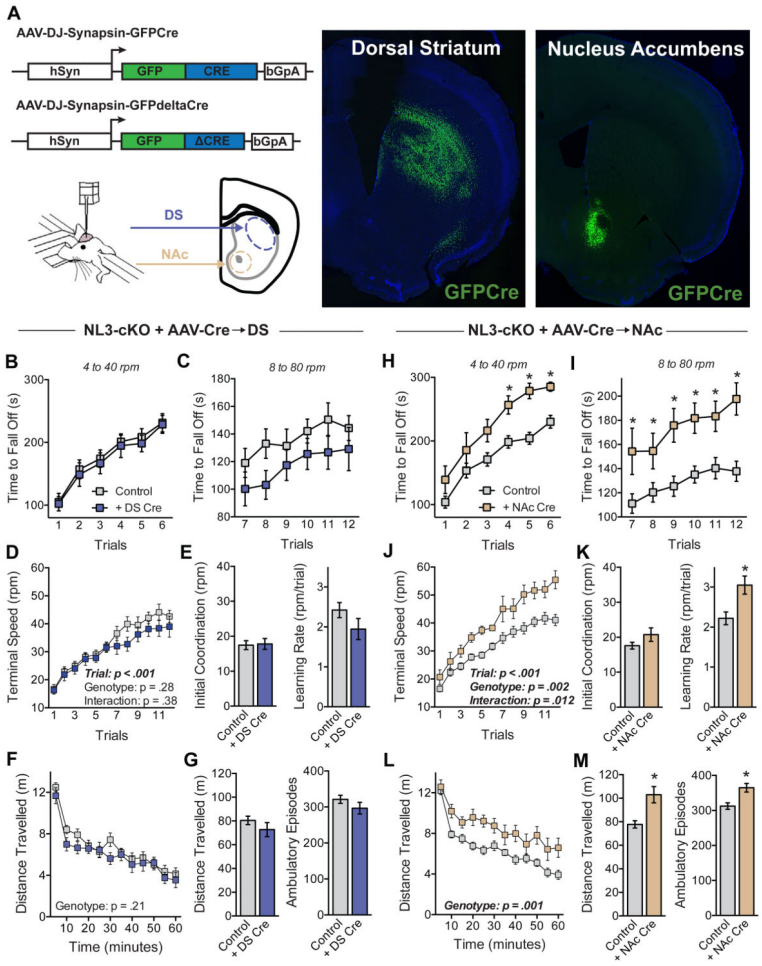

Figure 4. Conditional deletion of NL3 in the NAc but not the dorsal striatum causes enhanced rotarod learning

(A) Diagram of AAV constructs and stereotaxic injection of AAVs into the dorsal striatum (DS) or the NAc (left), and representative images showing GFP from viral injection localized to DS or NAc (right).

(B-E) Rotarod performance of NL3-cKO mice after injection of ΔCre (Control, n=15) or Cre into the DS (n = 11). Time to fall off is presented at *4 to 40 rpm* (B) and *8 to 80 rpm* (C); the terminal speed of rotation (D) was used to calculate initial coordination and learning rate (E).

(F & G) Behavior of the same mice in a test of open field activity, showing time course of activity across the entire session (F), as well as the total distance travelled and the number of ambulatory episodes (G).

(H-M) Behavior of control mice (n=26) and NL3-cKO mice receiving injection of Cre into NAc (n=9). For this comparison, the control group includes NL3-cKO mice receiving injection of ΔCre as well as injection of Cre into DS.

Data are means ± SEM; *significant difference between groups (ANOVA). Also see Figure S3.

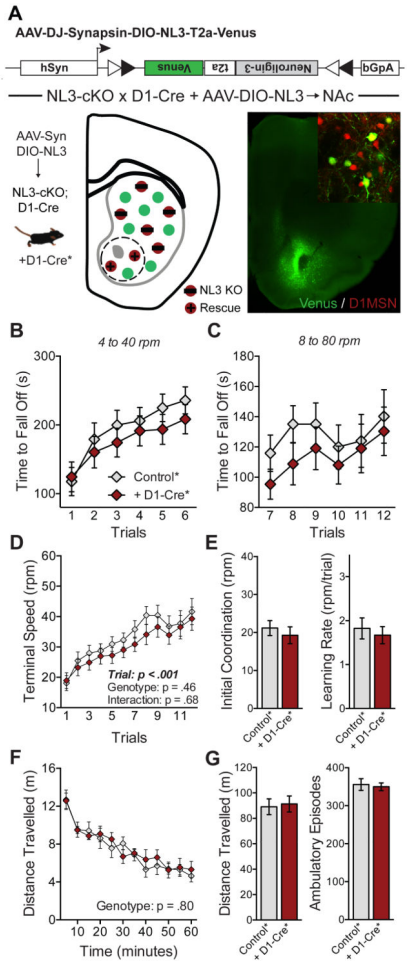

Figure 5. Behavioral phenotypes caused by NL3 loss-of-function are rescued by targeted expression of NL3 in D1-MSNs of the NAc

(A) Schematic of Cre-dependent NL3 rescue construct (DIO-NL3), with illustration of rescue in D1-MSNs of the NAc (lower left) and image of Venus expression in the NAc (lower right) as well as co-localization of rescue construct with D1 -tomato (inset).

(B-E) Rotarod performance of mice with DIO-NL3 injection in NAc, including a control group lacking Cre (n=10) and those carrying D1-Cre (n=9). Time to fall off is presented at *4 to 40 rpm* (B) and *8 to 80 rpm* (C); the terminal speed of rotation (D) was used to calculate initial coordination and learning rate (E).

(F and G) Behavior of the same mice in a test of open field activity, showing time course of activity across the entire session (F) as well as total distance travelled and number of ambulatory episodes (G).

Data are means ± SEM.

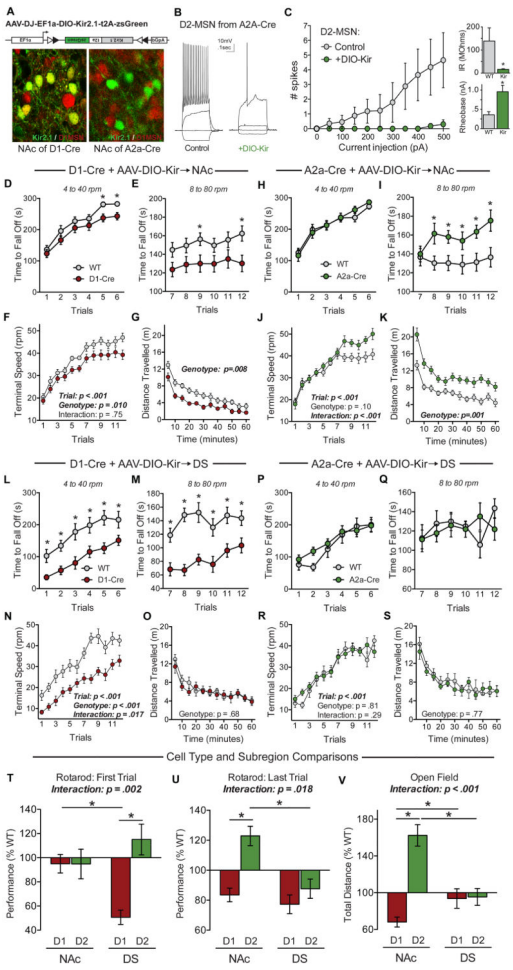

Figure 6. Subregion- and cell type-specific behavioral functions of D1- and D2-MSNs

(A) Schematic of Cre-dependent Kir2.1 construct (DIO-Kir), and confocal images from mice carrying D1-tomato showing co-localized expression in D1-Cre (lower left) and mutually exclusive expression in A2a-Cre (lower right).

(B and C) Examples of current-clamp recordings from uninfected (B, left) and infected (B, right) D2-MSNs in a double transgenic mouse carrying D1-tomato and A2a-Cre, and plot of the average number of spikes fired in response to a constant depolarizing current (C, left), as well as summary graphs of the average input resistance (IR) (C, upper right) and rheobase (C, lower right).

(D-F) Rotarod performance of WT (n=15) and D1-Cre mice (n=16) with DIO-Kir2.1 injections in the NAc, showing time to fall off at *4 to 40 rpm* (D) and *8 to 80 rpm* (E), as well as the terminal speed of rotation (F).

(G) Time course of open field activity in the same mice as D-F.

(H-K) Rotarod performance and open field activity of WT (n=12) and A2a-Cre mice (n=13) with DIO-Kir2.1 injections in the NAc.

(L-O) Rotarod performance and open field activity of WT (n=9) and D1-Cre mice (n=15) with DIO-Kir2.1 injection in the dorsal striatum (DS).

(P-S) Rotarod performance and open field activity of WT (n=7) and A2a-Cre mice (n=12) with DIO-Kir2.1 injection in the DS.

(T-V) Summary graphs comparing the effects of DIO-Kir2.1 in different striatal cell types and subregions. Data are presented as percentage of WT level on the first rotarod trial (T), last rotarod trial (U), and open field activity (V).

Data are means ± SEM; *significant difference between groups (ANOVA).

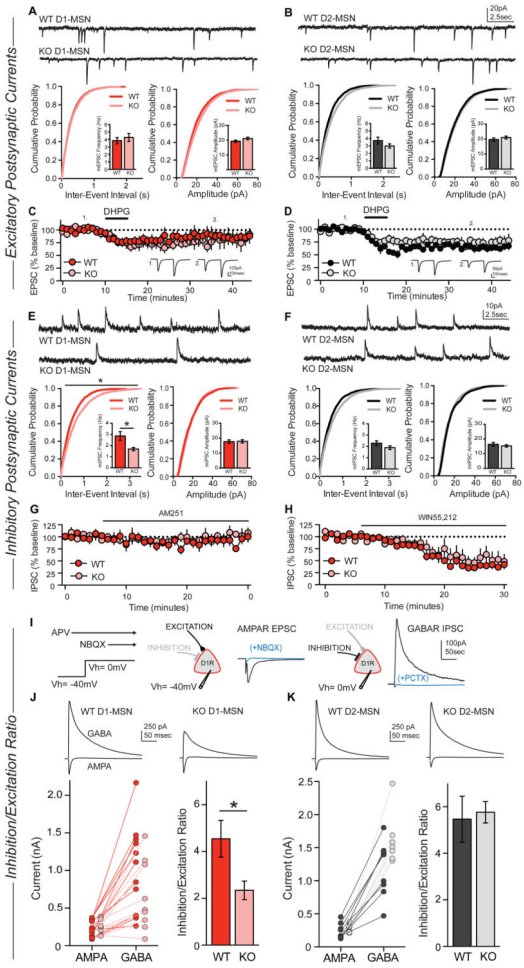

Figure 7. NL3 deletion decreases inhibitory synaptic transmission only in D1-MSNs but not D2-MSNs of the NAc

(A and B) Representative traces of mEPSCs in WT and NL3-KO cells (top), cumulative distribution of mEPSC inter-event intervals (lower left; inset shows average mEPSC frequency) and cumulative distribution of mEPSC amplitudes (lower right; inset shows average mEPSC amplitude) in WT (n=23) or NL3-KO (n=23) D1-MSNs (A), and WT (n=15) or NL3-KO (n=17) D2-MSNs (B).

(C and D) EPSC changes upon bath application of the group I mGluR agonist DHPG (100 μM), recorded in WT (n=7) or NL3-KO (n=6) D1-MSNs (C), and in WT (n=5) or NL3-KO (n=9) D2-MSNs (D).

(E and F) Representative traces, frequency, and amplitude of mIPSCs recorded in WT (n=17) or NL3-KO (n=17) D1-MSNs (E), and WT (n=12) or NL3-KO (n=15) D2-MSNs (F).

(G and H) Evoked IPSC amplitudes during bath application of the endocannabinoid receptor CB1 antagonist AM251 (2.5 μM) in WT (n=5) or NL3-KO (n=3) D1-MSNs (G), or during bath application of the CB1 agonist WIN55, 212 (1 μM) in WT (n=7) or NL3-KO (n=8) D1-MSNs (H).

(I) Illustration of the protocol used to measure the inhibition/excitation ratio.

(J and K) Representative traces of evoked AMPAR- and GABAR-mediated currents in WT or NL3-KO cells (top), amplitudes of AMPAR and GABAR currents (lower left), and average inhibition/excitation ratio (lower right) from WT (n=11) or NL3-KO (n=9) D1-MSNs (J), and WT (n=8) or NL3-KO (n=7) D2-MSNs (K).
Data are means ± SEM; *significant difference between groups (ANOVA). Also see Figures S5, S6 & S7.